Journal of Nuclear Materials 449 (2014) 219–224

Contents lists available at ScienceDirect

Journal of Nuclear Materials

journal homepage: www.elsevier.com/locate/jnucmat

Stability of self-interstitial clusters with C15 Laves phase structure in iron

L. Dézerald [a], M.-C. Marinica [a], Lisa Ventelon [a], D. Rodney [b], F. Willaime [a,*]

[a] CEA, DEN, Service de Recherches de Métallurgie Physique, F-91191 Gif-sur-Yvette, France
[b] Institut Lumière Matière, Université Lyon 1, CNRS, UMR 5306, F-69622 Villeurbanne, France

ARTICLE INFO

Article history:
Available online 13 February 2014

ABSTRACT

The energetics and stability of self-interstitial clusters with C15 Laves phase structure in iron are investigated by Density Functional Theory (DFT) calculations. First, the properties of bulk C15 are examined. The C15 structure is shown to be mechanically and dynamically stable. Second, the influence of the calculation scheme on the energy difference between C15, ring and loop configurations of di-, tri-, tetra- and octa-interstitial clusters is studied. These calculations confirm that, according to DFT, the C15 structure has by far the lowest energy of all known configurations of tetra- and octa-interstitial clusters in bcc-Fe.

1. Introduction

Point-defect clusters are formed in crystalline materials under irradiation either by clustering of point defects or directly in cascades in the case of irradiation by neutrons or high energy ions, as indicated by Molecular Dynamics (MD) simulations [1,2]. The defect morphology controls its migration kinetics, sink strength and dislocation-obstacle strength. For vacancy clusters there is a competition between planar loops and voids, and also stacking fault tetrahedra in face-centered cubic (fcc) metals. On the other hand, the observation of clusters of self-interstitial atoms (SIAs) in metals by transmission electron microscopy (TEM) techniques reveals only nanometer size planar loops. In body centered cubic (bcc) metals these loops have a 1/2 ⟨111⟩ Burgers vector, except in iron at high temperatures where it is ⟨100⟩ [3–5]. But the morphology adopted by SIA-clusters at small sizes – typically below a few tens of SIAs – is still largely debated. SIA clusters formed in MD simulations of cascades most often exhibit a morphology akin to dislocation loops. However, simulations in iron revealed that 30% to 50% of the clustered population of SIAs has a different morphology that renders them immobile, in contrast to the highly mobile 'glissile' loops [2]. The formation energies of SIA-clusters are a useful guide to indicate which configurations are likely to form, although other factors come into play because of the non-equilibrium character of their formation process. Quantitative insight into low energy structures of small SIA clusters in iron was gained from Density Functional Theory (DFT) calculations. Dumbbells can be packed together in bundles forming small dislocation loops. DFT predicts that in Fe the orientation of these dumbbells changes from ⟨110⟩ to ⟨111⟩ above around five SIAs [6]. Ring-type configurations, evidenced from empirical potential simulations [7,8], were found to have similar energies, or even lower for the di- and tri-interstitials, according to DFT: for the di-interstitial, a triangular ring with three atoms sharing the same site, for the tri-interstitial a hexagonal ring, and for the tetra-interstitial a hexagonal ring with a ⟨111⟩ crowdion perpendicular to it [8]. Recently, DFT calculations performed on SIA clusters containing up to 8 SIAs suggested that 3D clusters with a C15 Laves phase structure have much lower formation energies for clusters of 4 SIAs or more [9]. These clusters are observed in displacement cascade simulations performed over a wide range of primary knock-on atom energy, i.e. from 20 keV to 0.5 MeV [2,7,9,10]. These three families of SIA clusters are schematically represented in Fig. 1. We should note that 3D reconstructions are not limited to bcc metals nor to SIAs. For instance, clusters of 5 vacancies in aluminum adopt a specific configuration of very low relative energy [11,12], which corresponds to a local bcc unit cell in the fcc lattice.

In this paper, the properties of SIA clusters with C15 Laves phase structure are investigated by DFT calculations. The methodology of the DFT calculations is presented in Section 2. Then, the results on the stability of bulk C15 iron are presented through: (i) energy-volume curves; (ii) elastic constant calculations; and (iii) phonon dispersion curves. These three properties are important for C15 SIA-clusters because: (i) the formation energies of these clusters depend among others on the bcc-C15 energy difference and (ii)–(iii) a mechanical or dynamical instability of the C15 structure would prevent the existence of large C15 SIA

* Corresponding author. Tel.: +33 1 69 08 28 10.
E-mail address: francois.willaime@cea.fr (F. Willaime).

http://dx.doi.org/10.1016/j.jnucmat.2014.02.012
0022-3115/

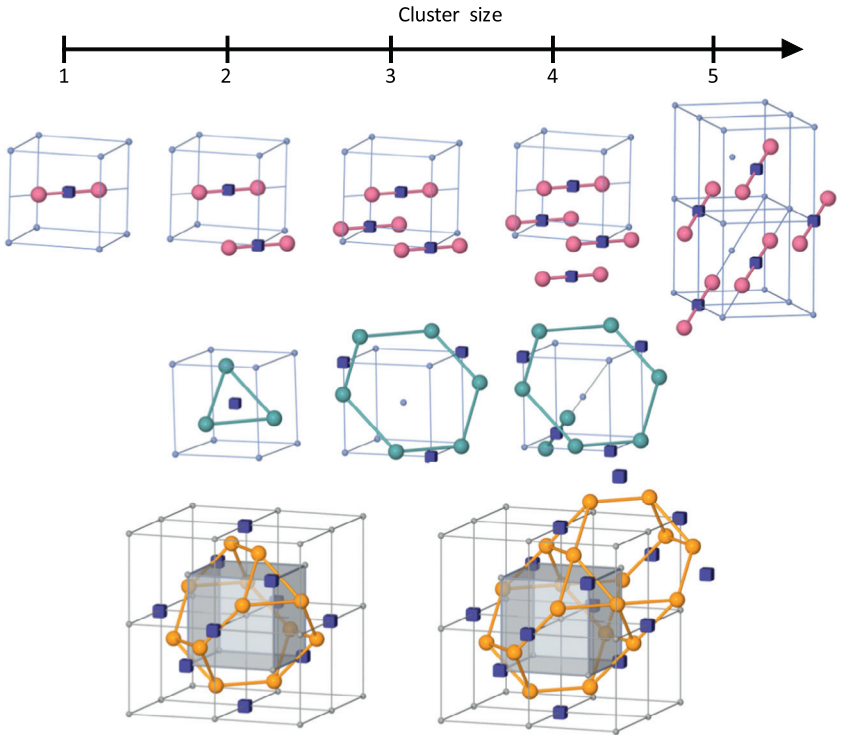

Fig. 1. Schematic representation of the various families of SIA clusters in bcc iron. Upper panel: parallel dumbbells aligned either in the ⟨1 1 0⟩ direction (up to 4 SIAs) or in the ⟨1 1 1⟩ direction (5 SIAs or more). Middle panel: ring-like structures (triangle or hexagons). Lower panel: C15-type clusters. The vacancies are represented by dark-blue cubes and the self-interstitial atoms by colored spheres. (For interpretation of the references to color in this figure legend, the reader is referred to the web version of this article.)

clusters. Finally, the formation energies of di-, tri-, tetra-, and octa-interstitials in the parallel dumbbell, ring and C15 configurations are compared for various calculations schemes.

2. Methodology

The DFT calculations are performed with the PWSCF code of the Quantum Espresso package [13] using ultrasoft pseudopotentials (USPP) or in the projector augmented wave (PAW) framework. The plane wave energy cutoff is 30 Ry for USPP and 40 Ry for PAW and the Hermite–Gaussian broadening-width for Brillouin zone integration is 0.3 eV. The calculations are performed either with 8 valence electrons (USPP and PAW) or including semi-core states with 16 valence electrons (denoted PAW-sc). For most calculations, the exchange correlation energy is evaluated using the Perdew–Burke–Ernzerhof (PBE) Generalized Gradient Approximation (GGA), but a few calculations are performed in the Local Density Approximation (LDA) for comparison although this functional is known to fail to reproduce the bcc ferromagnetic ground state for iron. Various magnetic states are compared, in particular for the C15 structure: ferromagnetic (FM), antiferromagnetic (AFM) or non magnetic (NM).

The bulk calculations are performed only with PAW-sc and GGA–PBE. The elastic constants are determined by finite difference, including the relaxation of internal degrees of freedom in the C15 structure. The phonon dispersions are evaluated using the Density Functional Perturbation Theory (DFPT) approach [14,15]. The *k*-point and *q*-point grids are $18 \times 18 \times 18$ and $8 \times 8 \times 8$ for bcc and $6 \times 6 \times 6$ and $3 \times 3 \times 3$ for C15, respectively. The augmentation charges are expanded up to 900 Ry for phonon calculations.

The supercell method was adopted for the defect calculations. Residual forces after relaxation are smaller than 0.01 eV/Å. The results presented here are obtained with 128+n or 250+n atom cells, where n is the number of SIAs, using a $3 \times 3 \times 3$ *k*-point grid. The convergence with supercell size of defect formation energies is often regarded as a limitation of DFT calculations. In practice, the formation energies in metals are generally observed to converge quite rapidly. Most defect DFT calculations in the literature are performed at fixed supercell volume, i.e. using for the defect supercell the same cell vectors as for the bulk supercell. This choice has obviously strong limitations when, as in the present case, the relative number of atoms between the two cells changes significantly. Relative formation energies can be affected by this choice if for instance two defects with different formation volumes are compared. Constant stress tensor conditions, using e.g. the Parrinello–Rahman algorithm, suffer from two limitations. First, these calculations are usually computationally much more demanding since they require a larger basis set in plane wave calculations in order to get converged values of the stress tensor components. Moreover, the local strain allowed by periodic boundary conditions does not correctly mimic that of a defect embedded in an infinite bulk matrix. We have therefore performed a comparison of the convergence with supercell size for four different conditions:

(i) constant supercell volume, where the shape and size of the supercell are fixed to that of the bulk equilibrium supercell;
(ii) constant rescaled volume, where the supercell is homogeneously rescaled from the bulk equilibrium supercell proportional to the number of atoms, i.e. for an octa-interstitial the cubic cell volume is fixed to $(N+8)\Omega_0$, where N is the number of the atoms in perfect crystal and Ω_0 is the equilibrium atomic volume;
(iii) constant pressure, with the trace of the stress tensor set to zero by homogenously rescaling the supercell;
(iv) constant stress, with all the components of the target stress tensor equal to zero.

The results obtained with the M07 EAM potential for iron [16] for the formation energies of two types of octa-interstitials in iron, namely the C15 and ⟨1 1 1⟩ parallel dumbbells, are displayed in

Fig. 2. In the C15 case, conditions (ii)-to-(iv) give almost identical results, which are clearly better converged at small sizes (128+8 and 250+8 atoms) than for constant supercell volume. For the more anisotropic case of ⟨1 1 1⟩ dumbbells, the convergence for (ii) and (iii) is also faster than for (i), but conditions (iv) show the largest deviation from the converged values at small sizes. It can be concluded that conditions (ii) and (iii) give identical results and that they are the most efficient conditions for obtaining both the absolute and relative values of the formation energies. Using 250+8 atom supercells, the deviation from the asymptotical limit of the formation energy is less than 2% for the C15 and 4% for the ⟨1 1 1⟩ dumbbells. Since conditions (ii), i.e. constant rescaled volume, are much easier to implement, we have performed all the present DFT calculations using these conditions. We should note that an alternative approach was proposed recently, based on constant volume calculations corrected for elastic interactions using the elastic dipole of the defect [17].

3. Results

3.1. Properties of bulk C15 iron and their impact on the stability of C15 SIA clusters

The energy-volume curves have been calculated for various structures and magnetic states. In addition to the conventional bcc, fcc (not shown) and hcp phases, we have also investigated the C15 cubic structure as well as A15, another cubic topologic close packed structure. A selection of the results is presented in Fig. 3. A15 and to a lesser extend C15 are known to be low energy structures in 4d and 5d transition metals of groups V and VI [18]. We find here that in iron also, these two structures in their ferromagnetic state are rather low in energy, 0.09 and 0.15 eV/atom above FM-bcc, respectively.

The low C15-bcc energy difference contributes to explain why the C15 structure is favorable for SIA clusters but a low interface energy and therefore a coherent interface with the bcc matrix are also needed. This therefore excludes hcp-type SIA clusters for instance. For cubic structures a small lattice mismatch with the bcc lattice is also required. Assuming that the equilibrium atomic volume is the same for all structures, one obtains that the lattice parameter of the C15 structure, $a_{C15} = 12^{1/3}\, a_{bcc} \approx 2.29\, a_{bcc}$. Therefore the lattice mismatch between C15 and a bcc double cell is only ~14%. For this reason it is possible to embed a coherent C15 Fe nanocrystal into a bcc Fe matrix. As a result – in the large size limit – a n-interstitial cluster is formed by replacing 2n atoms of the bcc lattice by 3n atoms displayed on a C15 lattice. If we now examine the A15 structure, which has a lower bulk energy than C15, $a_{A15} = 4^{1/3}\, a_{bcc} \approx 1.59\, a_{bcc}$. The 59% lattice mismatch between the two unit cells does not allow making a coherent interface between these 2 structures. Conversely the lattice mismatch between A15 and the bcc double cell, is −20%. The A15 structure is therefore a candidate for n-vacancy clusters where 2n bcc atoms are replaced by n A15 atoms. We have performed a few tests which show that these structures have higher energies than conventional vacancy

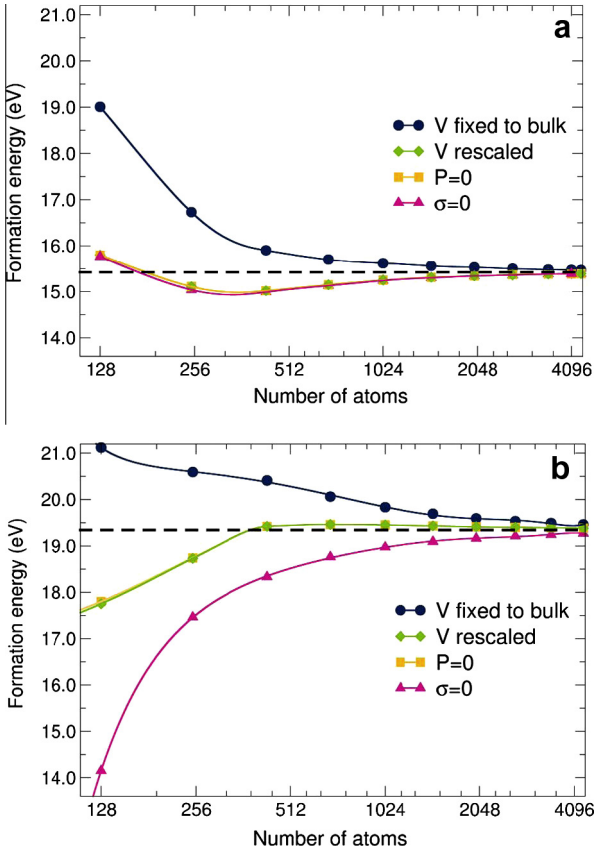

Fig. 2. Convergence with supercell size of the formation energies of 8 SIA clusters in bcc Fe. (a): C15 cluster. (b): ⟨1 1 1⟩ parallel dumbbells. The calculations are performed using the M07 EAM potential for iron at: (i) constant supercell volume (dark blue circles); (ii) constant rescaled volume (green diamonds); (iii) constant pressure (orange squares); and (iv) constant stress (magenta triangles). The dashed line shows the asymptotic limit, obtained using a 10^6 atom supercell. (For interpretation of the references to color in this figure legend, the reader is referred to the web version of this article.)

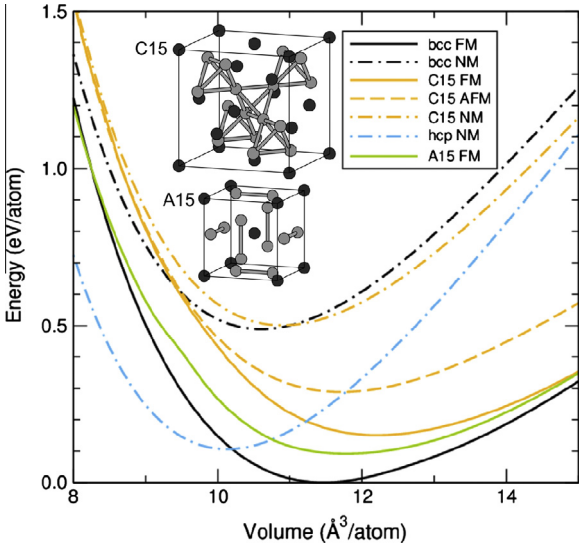

Fig. 3. DFT–GGA energy volume curves of various crystal structures in iron: comparison between the bcc (black), hcp (blue), A15 (green) and C15 (orange) structures, either in the non-magnetic (dash dot), ferromagnetic (continuous) or anti-ferromagnetic (dashed) state. (For interpretation of the references to color in this figure legend, the reader is referred to the web version of this article.)

Table 1
Bulk properties of bcc and C15 iron: lattice parameter (in Angströms) and elastic constants (in GPa). The DFT calculated values at 0 K are compared to experimental data in bcc-Fe (in parenthesis).

	a	B	C'	C_{44}
bcc	2.84 (2.87)	162 (168)[a]	68 (49)[a]	107 (116)[a]
C15	6.64	150	64	71

[a] Experimental data at 300 K [19].

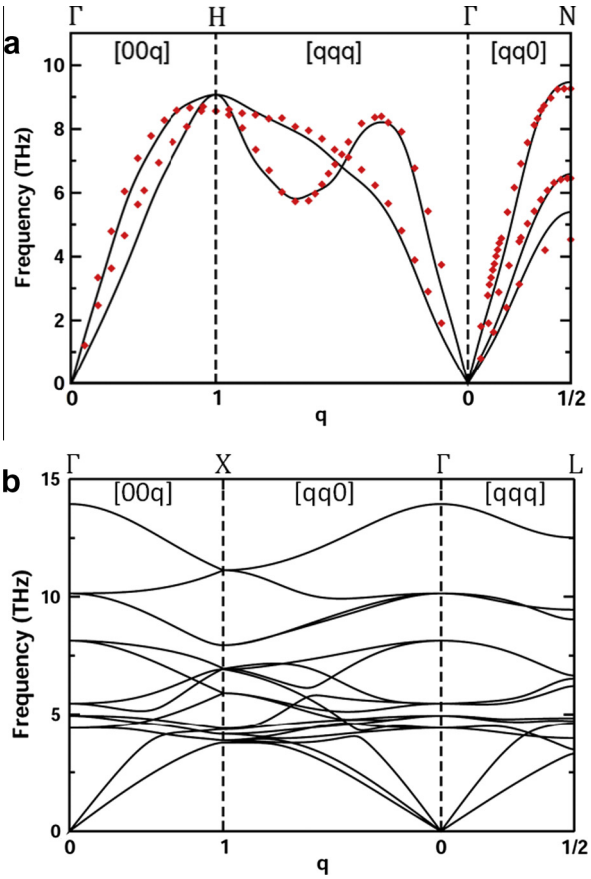

Fig. 4. Phonon dispersion along high symmetry directions in (a) bcc and (b) C15 iron. The lines correspond to DFT calculations and in (a) the symbols are experimental data measured at 300 K [22,23].

clusters. Finally, the fcc structure is also less favorable than C15 for interstitial clusters, with a larger lattice mismatch of 26%. In summary, what distinguishes C15 from other low-energy cubic structures is its sufficiently low lattice mismatch with respect to the bcc structures to allow for coherent interfaces between the two lattices.

This analysis may also explain why C15 SIA clusters have a lower energy in the AFM structure – with the exception of di- and tri-interstitials – than in the ferromagnetic structure which has a lower bulk energy. Since the AFM structure has a lower atomic volume, close to that of bcc, than the ferromagnetic structure (see Fig. 3), the elastic energy associated with this Eshelby inclusion is lower in the AFM structure, and this is proposed to compensate the larger bulk energy.

The lattice parameters and elastic constants of bcc and C15 iron in the ferromagnetic structure are displayed in Table 1. The bcc calculated values are in good agreement with experiments. The bulk modulus, B, is slightly smaller in C15 than in bcc. But most interestingly, C' and C_{44}, are both found to be positive, with values comparable to that of C' in the bcc structure. According to the Born stability criterion, the C15 structure is therefore stable against uniform deformations [20,21].

Finally, the phonon dispersion curves have been calculated in the high symmetry directions of the ferromagnetic bcc and C15 structures (Fig. 4). Since the C15 unit cell contains 6 atoms, up to 18 branches can be obtained in the absence of degeneracy. The results in bcc-Fe are in very good agreement with experimental data [22,23] and previous DFT calculations [24]. In the C15 structure, all vibration modes are found to be stable. The C15 structure is therefore predicted to be dynamically stable at ambient pressure and low temperature [21]. Note that optical modes with rather high frequencies compared to bcc are observed. Interestingly, similar high frequencies – in the range 10–15 THz – are observed for dumbbell rotation modes [25–27].

The mechanical and dynamical stability of the C15 lattice shows that this structure will not collapse at large SIA cluster sizes.

3.2. DFT formation energies of di-, tri-, tetra- and octa-interstitial clusters

Let us first recall the link between ring-type SIA structures and C15 SIA structures. The C15 structure for di-interstitials was initially obtained by combining the triangle and hexagonal ring low-energy building-blocks, as illustrated in Fig. 5. This construction illustrates the fact that closing the cage decreases the net number of additional atoms in the lattice from 3 to 2, therefore making a di-interstitial, as explained in Ref. [9]. The C15 tetra-interstitial is formed by 2 cages, as illustrated in Fig. 1.

Besides the usual considerations for defect calculations in metals using DFT, a particular attention has been paid in the present work on the initial magnetic moments set on the atoms for C15 defect structures. The self-consistent solution of the Kohn–Sham equations indeed depends in this case on the sign of the initial magnetic moments. Various combinations of initial distributions of magnetic moments have therefore been investigated. The general rule is that the lowest energies are obtained when the atoms of the cages, i.e. the interstitial atoms, and the atoms at the center of the cages have their spins opposite and aligned with respect to the bulk bcc atoms. The only exceptions are di- and tri-interstitials where both types of atoms of the clusters have their spins opposite to the bcc atoms. For di- and tri-interstitials if the spin of the central atom is reversed – so as to be aligned with the spin of bcc atoms – the energy increases by approximately 0.3 eV and the magnetic moment increases by 5 μ_B within both USPP and PAW GGA calculations. Bulk C15 being ferromagnetic, an interesting double inversion is observed as a function of cluster size: from ferromagnetic alignment for di- and tri-interstitials, to

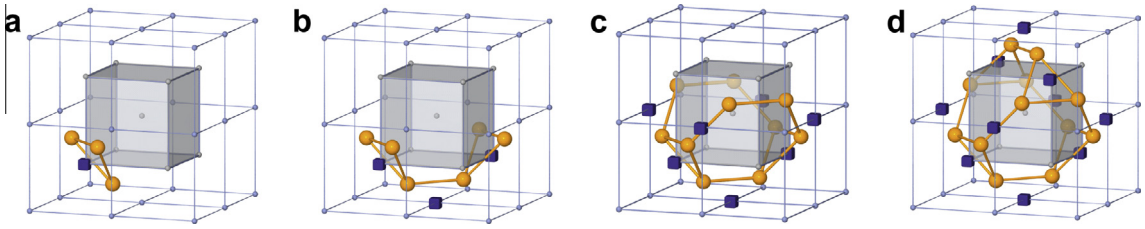

Fig. 5. Step by step geometrical construction of the C15 di-interstitial. (a): triangular di-interstitial formed by 3 SIAs (orange spheres) and one vacancy (blue cube). (b) tri-interstitial formed by 2 triangular di-interstitials and a vacancy, or equivalently 3 ⟨1 1 0⟩ dumbbells, i.e. 6 SIAs and 3 vacancies. (c): tri-interstitial with 10 SIAs and 7 vacancies. (d): C15 di-interstitial, with 12 SIAs and 10 vacancies. (For interpretation of the references to color in this figure legend, the reader is referred to the web version of this article.)

Table 2
Formation energies (in eV) and magnetic moments (in Bohr magnetons, μ_0) of the $\langle 1\,1\,0\rangle$ or $\langle 1\,1\,1\rangle$ parallel dumbbell, ring and C15 configurations of di-, tri-, tetra- and octa-interstitials (denoted I_2, I_3, I_4, and I_8 respectively) in bcc-Fe. The absolute formation energies are given for $\langle 1\,1\,0\rangle$ or $\langle 1\,1\,1\rangle$, and the formation energies relative to $\langle 1\,1\,0\rangle$ or $\langle 1\,1\,1\rangle$ are given for the ring and C15. Note that in LDA for the tetra-interstitial the $\langle 1\,1\,1\rangle$ dumbbell orientation is more stable than the $\langle 1\,1\,0\rangle$ one by 0.87 eV. The calculation scheme and number of atoms in the bulk supercell are indicated in the first and second column, respectively.

	N	$E_{I_2}^{\langle 1\,1\,0\rangle}$ $(\mu_{I_2}^{\langle 1\,1\,0\rangle}-\mu_{bulk})$	$E_{I_2}^{ring}-E_{I_2}^{\langle 1\,1\,0\rangle}$ $(\mu_{I_2}^{ring}-\mu_{bulk})$	$E_{I_2}^{C15}-E_{I_2}^{\langle 1\,1\,0\rangle}$ $(\mu_{I_2}^{C15}-\mu_{bulk})$	$E_{I_3}^{\langle 1\,1\,0\rangle}$ $(\mu_{I_3}^{\langle 1\,1\,0\rangle}-\mu_{bulk})$	$E_{I_3}^{C15}-E_{I_3}^{\langle 1\,1\,0\rangle}$ $(\mu_{I_3}^{C15}-\mu_{bulk})$	$E_{I_4}^{\langle 1\,1\,0\rangle}(\mu_{I_4}^{\langle 1\,1\,0\rangle}-\mu_{bulk})$	$E_{I_4}^{ring}-E_{I_4}^{\langle 1\,1\,0\rangle}$ $(\mu_{I_4}^{ring}-\mu_{bulk})$	$E_{I_4}^{C15}-E_{I_4}^{\langle 1\,1\,0\rangle}$ $(\mu_{I_4}^{C15}-\mu_{bulk})$	$E_{I_8}^{\langle 1\,1\,1\rangle}$ $(\mu_{I_8}^{\langle 1\,1\,1\rangle}-\mu_{bulk})$	$E_{I_8}^{C15}-E_{I_8}^{\langle 1\,1\,1\rangle}$ $(\mu_{I_8}^{C15}-\mu_{bulk})$
USPP	128	6.98 (−2.6)	−0.18 (−2.8)	+0.97 (−26.9)			12.44 (−6.3)	+0.16 (−8.16)	−1.47 (−38.0)		
USPP	250	7.08 (−2.9)	−0.10 (−2.8)	+0.78 (−32.0)	9.99 (−2.9)	+0.11 (−32.8)	12.72 (−6.2)	+0.16 (−7.19)	−1.29 (−38.9)	22.35 (−40.1)	−3.95 (−83.4)
PAW	250	7.55 (−2.6)	−0.10 (−3.0)	+0.79 (−31.6)	10.39 (−5.9)	+0.20 (−34.8)	13.60 (−6.8)	+0.16 (−9.22)	−1.83 (−39.9)	23.42 (−27.9)	−4.01 (−67.6)
PAW-sc	250	7.39 (−3.9)		+0.92 (−29.6)			13.32 (−5.6)		−1.23 (−35.5)		
USPP–LDA	128	6.81 (−12.2)	−0.43 (−15.8)	−1.76 (−36.8)			12.13 (−20.2)		−6.24 (−57.2)		

antiferromagnetic for 4 to 8 interstitials, and to ferromagnetic for bulk C15. The reason for the inversion at lower sizes is not clear.

The results of the formation energies of di-, tri-, tetra- and octa-interstitials, denoted I_2, I_3, I_4, and I_8 respectively, for the $\langle 1\,1\,0\rangle$ parallel dumbbell, ring-type and C15 configurations are summarized in Table 2. The change in magnetic moment is given with respect to the bulk supercell. The energy-difference discrepancies between 128 and 250 atom cells are small, i.e. at most 0.2 eV, as compared to the energy differences between the C15 and other structures. All GGA calculations, USPP or PAW, with or without semi-core states, yield very similar results, although for instance the C15- $\langle 1\,1\,0\rangle$ energy difference for the tetra-interstitial varies from −1.83 eV with PAW to −1.23 eV with PAW-sc. A significant scatter is also observed in the values of the magnetic moments. Both scatters are obviously strongly correlated: the lower the magnetic moment the lower the C15-cluster formation energy. A sharp contrast is observed in the LDA results: all magnetic moments are significantly lower, as well as the formation energies of the C15-clusters. We checked that this is not due to the instability of the bcc structure, i.e. the structure remains bcc in the calculation. Although LDA results in Fe must be taken with care, it is highly unusual to have such large discrepancies between LDA and GGA results.

All these results confirm and complete the findings of Ref. [9]:

- for di-interstitials, the lowest energy structure is the triangular ring within GGA and the C15 morphology within LDA,
- for tri-interstitials, the lowest energy structure is the hexagonal ring within GGA,
- for tetra-interstitials, the C15 structure is the most stable, 1.5 ± 0.3 eV below the $\langle 1\,1\,0\rangle$ parallel dumbbells within GGA and 5.4 eV below the $\langle 1\,1\,1\rangle$ parallel dumbbells within LDA,
- for octa-interstitials, the C15 structure is more stable than the $\langle 1\,1\,0\rangle$ parallel dumbbells by 4 eV.

In order to study the kinetics of C15 SIA clusters, using molecular dynamics or related methods, it is necessary to employ empirical potentials reproducing the properties predicted by DFT–GGA for these clusters. As outlined in Refs. [9,28] the C15-parallel dumbbell relative stabilities are highly dependent on the potential. For instance for the tetra-interstitials, the Ackland–Mendelev-2004 potential (AM04) [29] predicts an energy difference of 0.36 eV instead of 1.5 ± 0.3 eV according to DFT. The energy barrier needed to transform this immobile cluster into a mobile cluster is therefore largely underestimated using this potential [28]. To our knowledge the potential with highest fidelity for C15 cluster properties is the so-called M07 potential [16,9]. It reproduces much better the stability of the C15 tetra-interstitial relative to the $\langle 1\,1\,0\rangle$ parallel dumbbells, with a slight overestimation: 2.0 eV instead of 1.5 ± 0.3 eV according to DFT–GGA. The situation is even more favorable to this potential for octa-interstitials, with an energy relative to $\langle 1\,1\,1\rangle$ parallel dumbbells of 3.9 eV in excellent agreement with the DFT–GGA value, i.e. 4.0 ± 0.1 eV, against 0.7 eV for the AM04 potential.

4. Conclusion

In relation with the newly proposed C15-structure of SIA clusters in bcc-Fe, the properties of bulk C15 hypothetical crystals have been investigated by DFT–GGA calculations. The ground state of C15 is ferromagnetic, as for bcc. The C15 structure is shown to be 0.15 eV/atom higher in energy than bcc, with a slightly larger atomic volume and slightly smaller bulk modulus. The tetragonal and trigonal shear elastic constants, C' and C_{44}, are shown to be both positive, with values close to 60–70 GPa. The phonon dispersions of C15, calculated in the DFPT framework, attest for a

dynamical stability of the structure, in addition to the mechanical stability.

The properties of di-, tri-, tetra- and octa-interstitial clusters have then been investigated. First, we show that for this type of calculations, the constant rescaled volume approach is the most appropriate. All DFT–GGA calculations (USPP or PAW, with or without semi-core states) yield similar results for the formation energy differences between parallel dumbbells, ring-type (triangular or hexagonal) and C15 structures, and for their magnetic moments. In particular the exceptional stability of C15 tetra- and octa-interstitials and the large anti-ferromagnetic moments of C15-type SIA clusters are confirmed for all calculation schemes. These characteristics are even more pronounced within LDA.

Acknowledgment

This work was performed using HPC resources from GENCI-[CCRT/CINES] (Grant x2013096973).

References

[1] R.E. Stoller, G.R. Odette, B.D. Wirth, J. Nucl. Mater. 251 (1997) 49.
[2] D.J. Bacon, F. Gao, Y. Osetsky, J. Nucl. Mater. 276 (2000) 1.
[3] B.C. Masters, Nature 200 (1963) 254.
[4] S.L. Dudarev, R. Bullough, P.M. Derlet, Phys. Rev. Lett. 100 (2008) 135503.
[5] Z. Yao, M.L. Jenkins, M. Hernandez-Mayoral, M.A. Kirk, Philos. Mag. 90 (2010) 4623.
[6] F. Willaime, C.-C. Fu, M.-C. Marinica, J. Dalla Torre, Nucl. Instrum. Methods Phys. Res. Sect. B 228 (2004) 92.
[7] F. Gao, D.J. Bacon, Y.N. Osetsky, P.E.J. Flewitt, T.A. Lewis, J. Nucl. Mater. 276 (2000) 213.
[8] D.A. Terentyev, T.P.C. Klaver, P. Olsson, M.-C. Marinica, F. Willaime, C. Domain, L. Malerba, Phys. Rev. Lett. 100 (2008) 145503.
[9] M.-C. Marinica, F. Willaime, J.-P. Crocombette, Phys. Rev. Lett. 108 (2012) 025501.
[10] E. Zarkadoula, S.L. Daraszewicz, D.M. Duffy, M.A. Seaton, I.T. Todorov, K. Nordlund, M.T. Dove, K. Trachenko, J. Phys. Cond. Matter 25 (2013) 125402.
[11] H. Wang, D. Rodney, D.S. Xu, R. Yang, P. Veyssiere, Phys. Rev. B 84 (2011) 220103.
[12] H. Wang, D. Rodney, D.S. Xu, R. Yang, P. Veyssiere, Philos. Mag. 93 (2013) 186.
[13] P. Giannozzi et al., J. Phys. Condens. Matter 21 (2009) 395502.
[14] S. de Gironcoli, Phys. Rev. B 51 (1995) 6773.
[15] A. Dal Corso, Phys. Rev. B 81 (2010) 075123.
[16] L. Malerba et al., J. Nucl. Mater. 406 (2010) 19. see footnote [32] of Ref. [9] for a correction on one of the parameters.
[17] C. Varvenne, F. Bruneval, M.-C. Marinica, E. Clouet, Phys. Rev. B 88 (2013) 134102.
[18] B. Seiser, T. Hammerschmidt, A.N. Kolmogorov, R. Drautz, D.G. Pettifor, Phys. Rev. B 83 (2011) 224116.
[19] M.W. Guinan, D.N. Beshers, J. Phys. Chem. Solids 29 (1968) 541.
[20] M. Born, J. Chem. Phys. 7 (1939) 591.
[21] G. Grimvall, B. Magyari-Köpe, V. Ozolins, K.A. Persson, Rev. Modern Phys. 84 (2012) 945.
[22] V.J. Minkiewi, G. Shirane, R. Nathans, Phys. Rev. 162 (1967) 528.
[23] B.N. Brockhouse, H.E. Abouhela, E.D. Hallman, Solid State Commun. 5 (1967) 211.
[24] A. Dal Corso, S. de Gironcoli, Phys. Rev. B 62 (2000) 273.
[25] M.-C. Marinica, F. Willaime, Solid State Phen. 129 (2007) 67.
[26] S. Chiesa, P. Derlet, S. Dudarev, Phys. Rev. B 79 (2009) 214109.
[27] G. Lucas, R. Schäublin, Nucl. Instrum. Methods Phys. Res. Sec. B 267 (2009) 3009.
[28] H. Xu, R.E. Stoller, Y. Osetsky, J. Nucl. Mater. 443 (2013) 66.
[29] G.J. Ackland, M.I. Mendelev, D.J. Srolovitz, S. Han, A.V. Barashev, J. Phys. Condens. Matter 16 (2004) S2629.